AD-A125 023 MULTIAXIAL CREEP OF 2618 ALUMINUM UNDER PROPORTIONAL LOADING STEPS..(U) BROWN UNIV PROVIDENCE R I ENGINEERING MATERIALS RESEARCH LAB.. J DING ET AL. 1/1

UNCLASSIFIED NOV 82 EMRL-88 ARO-17741.2-EG F/G 11/6 NL

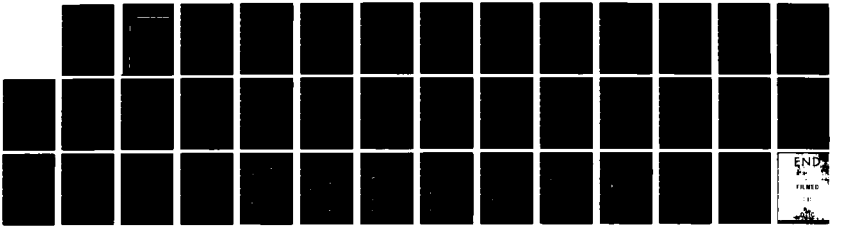

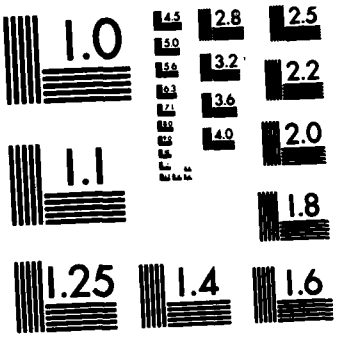

ARO 17741.2-EG (12)

Division of Engineering
BROWN UNIVERSITY
PROVIDENCE, R. I.

Engineering Materials Research Laboratory

MULTIAXIAL CREEP OF 2618 ALUMINUM UNDER PROPORTIONAL LOADING STEPS

Jow-Lian Ding

William N. Findley

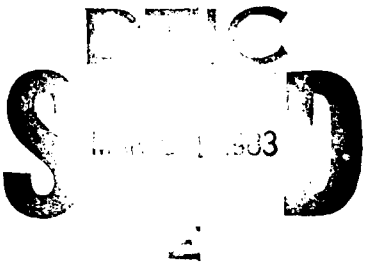

U.S. Army Research Office
Technical Report No. 2
Grant DAAG 29-81-K-0138

ARO DAAG 29-81-K-0138/2 *November 1982*
EMRL-88

UNCLASSIFIED
SECURITY CLASSIFICATION OF THIS PAGE (When Data Entered)

REPORT DOCUMENTATION PAGE		READ INSTRUCTIONS BEFORE COMPLETING FORM
1. REPORT NUMBER Technical Report No. 2	2. GOVT ACCESSION NO. AD-A125 028	3. RECIPIENT'S CATALOG NUMBER
4. TITLE (and Subtitle) "MULTIAXIAL CREEP OF 2618 ALUMINUM UNDER PROPORTIONAL LOADING STEPS".		5. TYPE OF REPORT & PERIOD COVERED Technical Rept.
		6. PERFORMING ORG. REPORT NUMBER EMRL-88
7. AUTHOR(s) Jow-Lian Ding and William N. Findley		8. CONTRACT OR GRANT NUMBER(s) Grant No. DAAG29-81-K-0138
9. PERFORMING ORGANIZATION NAME AND ADDRESS Division of Engineering, Brown University Box D, Providence, RI 02912		10. PROGRAM ELEMENT, PROJECT, TASK AREA & WORK UNIT NUMBERS
11. CONTROLLING OFFICE NAME AND ADDRESS U. S. Army Research Office Post Office Box 12211 Research Triangle Park, NC 27709		12. REPORT DATE November 1982 13. NUMBER OF PAGES 33 pages
14. MONITORING AGENCY NAME & ADDRESS(if different from Controlling Office)		15. SECURITY CLASS. (of this report) Unclassified 15a. DECLASSIFICATION/DOWNGRADING SCHEDULE

16. DISTRIBUTION STATEMENT (of this Report)

Approved for public release; distribution unlimited.

17. DISTRIBUTION STATEMENT (of the abstract entered in Block 20, if different from Report)

NA

18. SUPPLEMENTARY NOTES

The view, opinions, and/or findings contained in this report are those of the author(s) and should not be construed as an official Department of the Army position, policy, or decision, unless so designated by other documentation.

19. KEY WORDS (Continue on reverse side if necessary and identify by block number)

Multiaxial Creep; multistep creep; proportional loading; creep of aluminum alloy; strain hardening; kinematic hardening; viscous-viscoelastic model; viscoplastic model; transient creep.

20. ABSTRACT (Continue on reverse side if necessary and identify by block number)

Creep data of 2618-T61 aluminum alloy under multistep multiaxial proportional loadings at 200°C (392°F) are reported. Two viscoplastic flow rules were developed using constant stress creep and strain recovery data. One was based on the accumulated strain (strain hardening), and the other on a tensorial state variable (kinematic hardening). Data were represented by two models: a nonrecoverable viscoplastic model and a viscous-viscoelastic model in which the time-dependent strain was resolved into recoverable (viscoelastic) and

DD FORM 1 JAN 73 1473 EDITION OF 1 NOV 65 IS OBSOLETE

UNCLASSIFIED
SECURITY CLASSIFICATION OF THIS PAGE (When Data Entered)

#20. nonrecoverable components. The modified superposition principle was used to predict the viscoelastic strain component under variable stress states for both models. The experiments showed that the viscous-viscoelastic model with either strain-hardening or kinematic hardening gave very good predictions of the material responses. Strain hardening was best in some step-down stress states. The viscoelastic component accounted for not only the recovery strain but also the transient creep strain upon reloadings and step-up loadings.

Multiaxial Creep of 2618 Aluminum Under Proportional Loading Steps

by

Jow-Lian Ding[1]

and

William N. Findley[2]

[1]Research Assistant, Division of Engineering
Brown University, Providence, RI 02912

[2]Professor of Engineering, Division of Engineering
Brown University, Providence, RI 02912

U.S. Army Research Office
Technical Report No. 2
Grant DAAG-29-81-K-0138

Division of Engineering
Brown University
Providence, R.I. 02912

November 1982

Table of Contents

ABSTRACT

Creep data of 2618-T61 aluminum alloy under multistep multiaxial proportional loadings at 200°C (392°F) are reported. Two viscoplastic flow rules were developed using constant stress creep and strain recovery data. One was based on the accumulated strain (strain hardening), and the other on a tensorial state variable (kinematic hardening). Data were represented by two models: a nonrecoverable viscoplastic model; and a viscous-viscoelastic model in which the time-dependent strain was resolved into recoverable (viscoelastic) and nonrecoverable components. The modified superposition principle was used to predict the viscoelastic strain component under variable stress states for both models. The experiments showed that the viscous-viscoelastic model with either strain-hardening or kinematic hardening gave very good predictions of the material responses. Strain hardening was best in some step-down stress states. The viscoelastic component accounted for not only the recovery strain but also the transient creep strain upon reloadings and step-up loadings.

INTRODUCTION

There have been great advances in development of constitutive relations suitable for material used in design for high temperature. However, all suffer from a lack of experimental data to evaluate them [1].

Classically, most constitutive relations were based on the strain hardening rule. Some modifications have to be made for this approach to simulate the anisotropic nature observed in most structural materials, see [2,3] and [4, Chap. 2].

In recent theories state variables have been introduced to incorporate the anisotropic nature. The formulations usually consist of a flow rule which describes the interrelations between strain rate, applied stress, and state variables, and an evolution rule which describes the rate of change of the state variables with deformation and metallurgical effects. The evolution rule was generally based on the Bailey-Orowan model [5], and in most cases a tensorial state variable (back stress) was associated with the kinematic hardening nature and a scalar state variable with the isotropic hardening nature, see [6-8]. Nearly all theories used the Mises relation to extend their applicability from uniaxial to multiaxial stress states, and except for Hart's work [8], they are all based on the viscoplastic approach.

In previous work at Brown University on 2618-T61 aluminum [9-12], a viscous-viscoelastic model (VV) with strain hardening nature was developed and compared with a series of short term creep tests under various stress histories. The stress strain relations were refined in

[13] through a set of 48 hour creep and recovery data under constant multiaxial stress states including aging and compression tests. In current work, the previous strain hardening flow rule (SH) was refined and another kinematic hardening rule (KH) was derived from the stress strain relations reported in [13]. In addition to the VV model, a viscoplastic model (VP) in which all the time dependent strain was assumed nonrecoverable was also developed to show the role of the viscoelastic component. A set of 300-hour creep experiments under multiaxial multistep proportional loadings were compared with: a VV model with SH nature (VV-SH); a VV model with KH nature (VV-KH); a VP model with SH nature (VP-SH); and a VP model with KH nature (VP-KH). Future work will consider more complicated stress states such as nonproportional loadings, stress reversals and mixed stress relaxation and multiaxial creep.

MATERIAL, SPECIMEN, APPARATUS AND PROCEDURES

The material employed in the present work was aluminum alloy 2618-T61 which came from the same batch as that reported in [13], but probably different from that used in [9-12]. A more complete description of material and specimen were given in [9,13]. The combined tension and torsion machine and the compression machine used for these experiments were described in [14] and [15], respectively. The temperature control system and the data acquisition procedures were described in [9,14,15]. All the tests were performed at a test temperature of 200°C.

EXPERIMENTAL RESULTS

Eight tests are reported here whose loading programs and the resulting total strain versus time are shown in Fig. 1-8. The total duration of each test was around 300 h. The letter A preceeding the test number represents a pure tension or compression test, T represents a pure torsion test, and CA, CT represent the axial part and the torsion part, respectively, in a combined tension and torsion test. The first two steps of each test were constant stress creep followed by strain recovery. These were used for determining the stress-strain-time relations for constant stress states, as reported in [13]. Test 23, Fig. 1, was not shown in [13] because some friction was detected in the strain measuring system during the first step and small adjustments were made during step 2 to save the following steps.

The loading direction remains constant for each test. The stress magnitudes change abruptly in the following ways: step up followed by step down as in Fig. 2, step down followed by step up as in Fig. 3 and 8, and step down followed by reloading and step down as in Fig. 1, 4-7. Test A37, Fig. 7, is a compression test with the loading program exactly the same as that of tension test A32 shown in the same figure. The symmetry in tension and compression as discussed in [13] can be reaffirmed from Fig. 7. Another compression test is A44, Fig. 8.

The loading program for test 31 (CA31 or CT31), Fig. 5, 6 is basically the same as that for test A32 with equal magnitudes of effective stress defined by $\sigma^2 + 3\tau^2 = (\sigma_{eff})^2$ for each pair of corresponding steps.

The third step for all the tests except test A24 Fig. 2 was reloaded to the same stress as the first step. This always resulted

in some transient creep strain upon reloading to the previous creep stress level. Also all the step up steps resulted in transient creep. Partial unloading resulted in the following: If the reduction was small enough there was a period of strain recovery followed by new creep within 24 h or less, as in period 6 Fig. 1 and 2, period 4 Fig. 3, period 7 Fig. 5, 6 and 7. However, in period 4 Fig. 8 a reduction of stress similar to that of period 4 Fig. 3 but at much higher stress yielded continuous strain recovery during the period of observation.

When the stress was reduced in one or two steps to about one half there was a short strain recovery period followed by a long period with no strain change, as in period 7 Fig. 1 and 2, period 4 Fig. 4, 5, 6, and 7, period 7 Fig. 4, and period 9 Fig. 8. If the stress was reduced in several steps to a sufficiently small proportion of the initial stress, continuous slow strain recovery was observed as in period 8 Fig. 1, 6 and 7, period 5 Fig. 3 and 8.

STRESS-STRAIN-TIME RELATIONS FOR CONSTANT STRESS STATES

In the VV model, the total strain ε_{ij} during constant stress creep was represented as:

$$\varepsilon_{ij} = \varepsilon_{ij}^{E} + \varepsilon_{ij}^{+VE} t^{n_1} + \varepsilon_{ijt}^{+V} t^{n_2} , \qquad (1)$$

where ε_{ij}^{E} is the time independent elastic strain, $\varepsilon_{ij}^{+VE} t^{n_1} = \varepsilon_{ij}^{VE}$ is the viscoelastic component, and $\varepsilon_{ijt}^{+V} t^{n_2} = \varepsilon_{ij}^{V}$ is the time dependent nonrecoverable component for the VV model. n_1 and n_2 are 0.223 and 0.496, respectively, see [13]. Time independent plastic strain was

negligible for this material at the stresses employed. In the VP model, the total strain ϵ_{ij} during creep is

$$\epsilon_{ij} = \overset{E}{\epsilon}_{ij} + \overset{+}{\epsilon}_{ij}t^N \quad , \tag{2}$$

where $\overset{+}{\epsilon}_{ij}t^N = \overset{v}{\epsilon}_{ij}$ is the time dependent strain for the VP model, and N was found to be 0.407, [13]. The elastic moduli for tension E and for torsion G were found to be 6.50×10^4 MPa (9.43×10^3 ksi) and 2.38×10^4 MPa (3.45×10^3 ksi), respectively. The third order multiple integral representation yields the following expressions for the stress dependent coefficients ϵ_{11}^{+VE} and ϵ_{12}^{+VE} under constant combined tension and torsion stress, i.e.,

$$\epsilon_{11}^{+VE} = F^{VE}(\sigma,\tau) = \overset{+}{F}_1\sigma + \overset{+}{F}_3\sigma^3 + \overset{+}{F}_4\sigma\tau^2 \quad , \tag{3}$$

$$\epsilon_{12}^{+VE} = G^{VE}(\sigma,\tau) = \overset{+}{G}_1\tau + \overset{+}{G}_2\tau^3 + \overset{+}{G}_4\sigma^2\tau \quad , \tag{4}$$

where $\overset{+}{F}_i$ and $\overset{+}{G}_i$ are constants whose values are given in [13].

A function F_a (or F_b)of maximum shear stress τ_{max} multiplied by the stress deviator σ'_{ij}, was developed to represent the stress dependence of ϵ_{ij}^{+V} or $\overset{+}{\epsilon}_{ij}$ as follows,

$$\epsilon_{ij}^{+V} = \sigma'_{ij}F_a(\tau_{max}) \quad , \tag{5}$$

where

$$F_a(\tau_{max}) = 3.616 \times 10^{-5} \times \{1 + 0.3914 \times \exp[2.108 \times 10^5 \times (\tau_{max}/G)^2]\} \quad ,$$

percent per MPa-hr$^{0.496}$,

and

$$\dot{\varepsilon}_{ij}^{+} = \sigma'_{ij} F_b(\tau_{max}) \quad , \tag{6}$$

where

$$F_b(\tau_{max}) = 6.219 \times 10^{-5} \times \{1 + 0.6433 \times \exp[1.633 \times 10^5 \times (\tau_{max}/G)^2]\} \quad ,$$

percent per MPa-hr$^{0.407}$,

where G is the shear modulus. Equations (5) and (6) represent the data best of several different formulations considered, such as power function, hyperbolic sine and combinations of power and exponential functions.

WEAKENING EFFECTS

In previous work [13], secondary and tertiary creep stages were observed when the magnitude of the effective stress was 137.2 MPa (19.90 ksi) or higher. It was also reported that there were no significant aging effects in this precipitation hardened material in 300 hours. The onset of the secondary and tertiary stages could be caused by a combination of several other weakening effects such as static recovery, dynamic recovery, grain boundary shearing and intercrystalline fracture. In current work, these possible weakening effects were neglected in the theoretical analysis, which did not consider the occurrence of secondary and tertiary stages.

CONSTITUTIVE EQUATIONS FOR VARIABLE STRESS STATES

VISCOELASTIC STRAIN, ε_{ij}^{VE}: By the modified superposition principle [9, 16, 17] the viscoelastic strain for a varying stress is given by

$$\varepsilon = \int_0^t \frac{\partial f[\sigma(\xi), t-\xi]}{\partial \sigma(\xi)} \dot{\sigma}(\xi) d\xi \quad , \tag{7}$$

where the strain at constant stress is given by $\varepsilon = f(\sigma,t)$.

For a series of m steps in stress as in the present test programs, the strain was described by the following form from Eq. (7)

$$\begin{aligned} \varepsilon_{11}^{VE} &= F^{VE}(\sigma_1,\tau_1)[t^{n_1} - (t-t_1)^{n_1}] + \ldots \\ &+ F^{VE}(\sigma_{m-1},\tau_{m-1})[(t-t_{m-2})^{n_1} - (t-t_{m-1})^{n_1}] \\ &+ F^{VE}(\sigma_m,\tau_m)(t-t_{m-1})^{n_1} \quad , \quad t_{m-1} < t \quad . \end{aligned} \tag{8}$$

Similarly, ε_{12}^{VE} was obtained by replacing $F^{VE}(\sigma,\tau)$ by $G^{VE}(\sigma,\tau)$ in Eq. (8).

TIME DEPENDENT NONRECOVERABLE STRAIN, ε_{ij}^{V}: Two flow rules, strain hardening or kinematic hardening, were developed here for ε_{ij}^{V} under variable stress states. The derivation was based on the assumption that the hardening nature of the material under variable stress states was the same as that under constant stress states.

DEVELOPMENT OF THE STRAIN HARDENING FLOW RULE: Here only the case for the ε_{ij}^{V} (VP model) is discussed. The derivations are exactly the same for the ε_{ij}^{V} (VV model) except for different values for the time exponents and different relationships for $F(\tau_{max})$.

As shown in [13], ε_{ij}^{V} under constant stress creep can be expressed as:

$$\varepsilon_{ij}^{V} = F(\tau_{max})\sigma'_{ij}t^{N} \quad . \tag{9}$$

Differentiating both sides with respect to time yields

$$\dot{\varepsilon}_{ij}^{V} = NF(\tau_{max})\sigma'_{ij}t^{N-1} \quad . \tag{10}$$

To obtain a strain hardening flow rule the t in Eq. (10) was expressed in terms of the accumulated strain as follows. Taking the maximum of the shear strain on the left hand side of Eq. (9) and the maximum of the shear stress on the right hand side yields the following expression:

$$\overline{\varepsilon_{ij}^{V}} = \tau_{max}F(\tau_{max})t^{N} \quad , \tag{11}$$

from which,

$$t = \{\overline{\varepsilon_{ij}^{V}}/[\tau_{max}F(\tau_{max})]\}^{1/N} \quad , \tag{12}$$

where $\overline{\varepsilon_{ij}^{V}}$ is the magnitude of the strain tensor defined by the Tresca relation. The choice of the Tresca relation instead of a Mises

relation for magnitude quantities came from the observation that the maximum shear rates are constant at any given time for those creep tests whose stress levels are the same according to the Tresca relation as discussed in [13]. For combined tension σ and torsion τ stress states, τ_{max} is equal to $[(\sigma/2)^2+\tau^2]^{1/2}$ and $\overline{\varepsilon^V_{ij}}$ equals $\{[(3/4)\varepsilon^V_{11}]^2+(\varepsilon^V_{12})^2\}^{1/2}$. Substituting t from Eq. (12) into Eq. (10) yielded the strain hardening flow rule,

$$\dot{\varepsilon}^V_{ij} = \sigma'_{ij} NF(\tau_{max})\{\overline{\varepsilon^V_{ij}}/[\tau_{max}F(\tau_{max})]\}^{(N-1)/N}, \qquad (13)$$

where $F(\tau_{max})$ is as follows: For the VP model, $F(\tau_{max})$ is $F_b(\tau_{max})$, Eq. (6). For the VV model, N is replaced by n_2 and $F(\tau_{max})$ is $F_a(\tau_{max})$, Eq. (5).

Furthermore, differentiating both sides of Eq. (11) with respect to time t, substituting Eq. (12) for t and dividing by $\overline{\varepsilon^V_{ij}}$ yields

$$\dot{\overline{\varepsilon^V_{ij}}}/[(\overline{\varepsilon^V_{ij}})^{(N-1)/N}] = N[\tau_{max}F(\tau_{max})]^{1/N} \quad . \qquad (14)$$

Integrating (14) with respect to time yields

$$\overline{\varepsilon^V_{ij}} = \{\int_0^t [\tau_{max}(\xi)F(\tau_{max}(\xi))]^{1/N} d\xi\}^N \quad . \qquad (15)$$

For a series of m steps in stress, Eq. (15) becomes

$$\begin{aligned}\overline{\varepsilon^V_{ij}} = {} & \{[\tau_{max(1)}F(\tau_{max(1)})]^{1/N}(t_1) + \ldots \\ & + [\tau_{max(m-1)}F(\tau_{max(m-1)})]^{1/N}(t_{m-1}-t_{m-2}) \\ & + [\tau_{max(m)}F(\tau_{max(m)})]^{1/N}(t-t_{m-1})\}^N \quad , \quad t_{m-1} < t \quad . \qquad (16)\end{aligned}$$

Eq. (16) is true for both proportional and nonproportional loadings. However, for proportional loadings, the strain components at any given time can be obtained directly from Eq. (16) because the loading direction is constant throughout the test. From Eq. (13) a constant loading direction implies constant strain rate direction and thus constant strain direction. In the combined tension σ and torsion τ stress states σ'_{ij} is equal to zero except $\sigma'_{11} = (2/3)\sigma$, $\sigma'_{22} = \sigma'_{33} = (-1/3)\sigma$, and $\sigma'_{12} = \sigma'_{21} = \tau$. In multistep proportional loadings, $\tau/[(2/3)\sigma] = \varepsilon^v_{12}/\varepsilon^v_{11} = k$, where k is a constant for each test, and $\overline{\varepsilon^v_{ij}}$ and τ_{max} can be expressed as:

$$\overline{\varepsilon^v_{ij}} = \{[(3/4)\varepsilon^v_{11}]^2 + (\varepsilon^v_{12})^2\}^{1/2} = \varepsilon^v_{11}(k^2+(9/16))^{1/2} , \qquad (17)$$

$$\tau_{max} = [(\sigma/2)^2+\tau^2]^{1/2} = [(2/3)\sigma](k^2+(9/16))^{1/2} . \qquad (18)$$

By substituting (17) and (18) into (16) ε^v_{11} under a series of m steps in stress can be obtained as

$$\varepsilon^v_{11} = \{[(2\sigma_1/3)\, F(\tau_{max(1)})]^{1/N} (t_1) + \ldots$$

$$+ [(2\sigma_{m-1}/3)\, F(\tau_{max(m-1)})]^{1/N} (t_{m-1} - t_{m-2})$$

$$+ [(2\sigma_m/3)\, F(\tau_{max(m)})]^{1/N} (t-t_{m-1})\}^N , \quad t_{m-1} < t . \qquad (19)$$

A similar form can be obtained for ε^v_{12} with $2\sigma/3$ replaced by τ. The above expressions are exactly the same as those reported in [10,16] with the stress dependent coefficients replaced by $F(\tau_{max})\sigma'_{ij}$.

DEVELOPMENT OF THE KINEMATIC HARDENING FLOW RULE: Neglecting the weakening effects mentioned in a previous paragraph, a general form of the kinematic hardening model can be expressed as:

$$\dot{\varepsilon}^{V}_{ij} = [H_1(|\Sigma_{ij}|)]\Sigma_{ij}/|\Sigma_{ij}| \quad \text{(flow rule)} \ , \tag{20}$$

and

$$\dot{\alpha}_{ij} = H_2(|\alpha_{ij}| \ , |\dot{\varepsilon}^{V}_{ij}|)\dot{\varepsilon}^{V}_{ij} \quad \text{(evolution rule)} \ , \tag{21}$$

where $\Sigma_{ij} = \sigma'_{ij} - \alpha_{ij}$, σ'_{ij} is the stress deviator, α_{ij} is the state variable (back stress), and $|\Sigma_{ij}|$, $|\alpha_{ij}|$, $|\dot{\varepsilon}_{ij}|$ are the magnitudes of the corresponding stress tensors, which in principle can be defined by either Mises or Tresca relations, see [6-8]. By symmetry in tension and compression and the indifference of creep strain to the stress direction, as implied by Eq. (3) and (6), it is reasonable to assume the initial values of α_{ij} are all zero.

In a pure torsion test, σ'_{ij} is equal to zero except for $\sigma'_{12} = \sigma'_{21} = \tau$, which implies, according to Eq. (20) and (21), that all the tensorial components are zero except for $\dot{\varepsilon}^{V}_{12} = \dot{\varepsilon}^{V}_{21} \neq 0$, $\dot{\alpha}_{12} = \dot{\alpha}_{21} \neq 0$, $\varepsilon_{12} = \varepsilon_{21} \neq 0$, $\alpha_{12} = \alpha_{21} = \alpha \neq 0$, and that $|\Sigma_{ij}|$, $|\alpha_{ij}|$ and $|\dot{\varepsilon}^{V}_{ij}|$ are equal to $|\tau-\alpha|$, $|\alpha|$, and $|\dot{\varepsilon}^{V}_{12}|$, respectively. Eq. (20) and (21) thus reduce to the following forms:

$$\dot{\varepsilon}^{V}_{12} = H_1(\tau-\alpha) \ , \tag{22}$$

$$\dot{\alpha}_{12} = H_2(\alpha, \dot{\varepsilon}^{V}_{12})\dot{\varepsilon}^{V}_{12} \ . \tag{23}$$

Since the initial value of α is zero, the initial shear creep rate is a function of shear stress only, according to Eq. (22), i.e., $\dot{\varepsilon}^{V}_{12(t=0)} = H_1(\tau)$. Therefore function H_1 can be specified by the relationship between the initial shear creep rates and shear stresses.

However, the initial creep rates are so rapid as to be indeterminant, possibly infinite according to Eq. (1), (2). In order to obtain a reasonable estimation of an initial creep rate, the first two hours of creep data of all the tests reported in [13] were fitted by Eq. (1) with $n_1 = 0.223$ to obtain n_2 for use in ε^{V}(VV model) and by Eq. (2) to obtain N for use in ε^{V} (VP model). In [13] Eq. (2) was used to fit the first two hours of creep data to get ε^{o}_{ij} for the determination of the elastic moduli.

It was found that there existed small gaps between ε^{o}_{ij} and the estimated elastic responses for some high stress level creep tests. These gaps might be due to plastic strain or high strain rate effects during loading. These gaps were neglected and no time independent plastic strain was included in the theoretical analysis, see [13]. To compensate for these gaps by time dependent strain, a virtual data at t = 0 calculated from E or G was put in each of those creep data sets whose effective stress magnitudes were equal to or greater than 137.2 MPa (19.90 ksi) as mentioned in the note for Table 3 in [13]. Since the deviations were small they actually had very little effect on the data fittings. The averages of n_2 and N are 0.330 and 0.292 respectively. Because only the values of ε^{+V}_{ij} and ε^{+}_{ij} with n_2 and N fixed are involved in the creep rate estimations, the values of n_2 and N for individual tests are not shown here.

Refitting the 2-hour data by Eq. (1) and (2) with n_2 and N fixed yields the values of ε_{ij}^{+V} in Eq. (1) and ε_{ij}^{+} in Eq. (2) which are shown in Table 1. Instead of the initial creep rate (infinite) an "early" value of creep rate was used in determining H_1. The "early" creep rates were calculated either by $n_2\varepsilon_{ij}^{+V}t_1^{n_2-1}$ (or $N\varepsilon_{ij}^{+}t_1^{N-1}$) or by $\varepsilon_{ij}^{+V}t_1^{n_2}/t_1$ (or $\varepsilon_{ij}^{+}t_1^{N}/t_1$), where t_1 is a small time such as 1 sec. In either case it can be seen that the ratios of creep rates for different tests depend only on ε_{ij}^{+V} or ε_{ij}^{+}. Different approaches or choices of t_1 can only result in a different constant multiplier for H_1 whose effect will be discussed in a later section. The initial creep rates based on the first approach with t_1 = 1 sec. are shown in Table 1.

The relationships between "initial" shear creep rates and τ were found to be best represented by the following expressions:
For the VV model,

$$\dot{\varepsilon}_{12(t=0)}^{V} = C_1\sinh(\tau/K_1) \quad , \tag{24}$$

or, for the VP model,

$$\dot{\varepsilon}_{12(t=0)}^{V} = C_2\sinh(\tau/K_2) \quad , \tag{25}$$

where K_1, K_2 are 19.34 MPa (2.805 ksi) and 22.23 MPa (3.225 ksi) respectively; and C_1, C_2 are equal to 0.06371 and 0.1929 in percent/h, respectively, see Fig. 9.

According to Eq. (20) and (22) the flow rules for pure torsion loadings can then be expressed as:

$$\dot{\varepsilon}^{V}_{12}(t) = C_1 \sinh [(\tau-\alpha)/K_1] \quad , \quad (VV) \quad , \tag{26}$$

or

$$\dot{\varepsilon}^{V}_{12}(t) = C_2 \sinh [(\tau-\alpha)/K_2] \quad , \quad (VP) \quad . \tag{27}$$

To obtain the evolution rule, an interrelation between $\dot{\alpha}$, α, and $\dot{\varepsilon}^{V}_{12}$ during deformation was derived from constant stress shear creep tests. Here, ε^{V}(VP Model) is used as an example; the same method applies for ε^{V}(VV Model) except for different constants. From Eq. (27) it follows that: for any stress histories,

$$\tau-\alpha = K_2 \ln\{(\dot{\varepsilon}^{V}_{12}/C_2) + [(\dot{\varepsilon}^{V}_{12}/C_2)^2 + 1]^{1/2}\} \quad . \tag{28}$$

For pure torsion creep tests in which τ is constant, differentiating Eq. (28) with respect to time yields:

$$\dot{\alpha} = -K_2 \ddot{\varepsilon}^{V}_{12}/[(\dot{\varepsilon}^{V}_{12})^2 + C_2^2]^{1/2} \quad . \tag{29}$$

The evolution rule can be obtained by expressing $\ddot{\varepsilon}^{V}_{12}$ in Eq. (29) in terms of α and $\dot{\varepsilon}^{V}_{12}$. Recalling that the creep strain can be expressed by $\varepsilon^{V}_{12} = \varepsilon^{+}_{12} t^N$ in the VP model, the following results were obtained by consecutive differentiation with respect to time:

$$\dot{\varepsilon}^{V}_{12} = N \varepsilon^{+}_{12} t^{N-1} \quad , \tag{30}$$

$$\ddot{\varepsilon}^{V}_{12} = N(N-1) \varepsilon^{+}_{12} t^{N-2} \quad . \tag{31}$$

From (30) and (31),

$$\ddot{\varepsilon}_{12}^{V} = [(N-1)/t]\dot{\varepsilon}_{12}^{V}$$

$$= (N-1)(\varepsilon_{12}^{+}N)^{1/(N-1)}(\dot{\varepsilon}_{12}^{V})^{-1/(N-1)}\dot{\varepsilon}_{12}^{V} \quad . \qquad (32)$$

ε_{12}^{+} in Eq. (32) is equal to $\tau F_b(\tau)$ according to Eq. (6). Substituting τ from Eq. (28) makes $\ddot{\varepsilon}_{12}^{V}$ in (32) a function of α and $\dot{\varepsilon}_{12}^{V}$ only. Introducing Eq. (32) into Eq. (29) yields the evolution rule; i.e., the relation between $\dot{\alpha}$, α and $\dot{\varepsilon}_{12}^{V}$ during creep. Even though the evolution rule for hardening was derived from creep tests at constant stress it was assumed that the same hardening nature would be applicable for other stress histories.

For the VV model the evolution rule is the same as the VP model except N is replaced by n_2 and ε_{12}^{+} is replaced by $\varepsilon_{12}^{+V} = \tau F_a(\tau)$ from Eq. (5).

Since Eq. (27) and (29) (with Eq. (32) inserted in Eq. (29)) were both derived from constant stress creep tests, the kinematic hardening rule, Eq. (27) and (29), describe the creep curves very well regardless of values of C_1 (or C_2) employed. But different values of C_1 (or C_2) result in different values of α during creep according to Eq. (28). However, $\dot{\varepsilon}_{12}^{V}$ in Eq. (28) is very small compared to C_1 (or C_2) except at the very beginning of a test. Thus differences in C_1 (or C_2) are generally unimportant.

Isotropic hardening effects can be taken into consideration, if required, by developing an evolution rule for K_1 (or K_2) as in [6,7].

KINEMATIC HARDENING RULES FOR MULTIAXIAL STRESS STATES

Equation (27), (29) and (32) can be extended to multiaxial stress states as follows. For ε^{V}_{ij}, (VP Model),

$$\dot{\varepsilon}^{V}_{ij} = C_2(\Sigma_{ij}/|\Sigma_{ij}|)\sinh(|\Sigma_{ij}|/K_2) \quad , \tag{33}$$

$$\dot{\alpha}_{ij} = -\frac{K_2(N-1)(b_1N)^{1/(N-1)}|\dot{\varepsilon}^{V}_{ij}|^{-1/(N-1)}}{(|\dot{\varepsilon}^{V}_{ij}|^2 + C_2^2)^{1/2}}\dot{\varepsilon}^{V}_{ij} \quad , \tag{34}$$

where $b_1 = b_2F_b(b_2)$ and

$$b_2 = |\alpha_{ij}| + K_2\,\ell_n\{(|\dot{\varepsilon}^{V}_{ij}|/C_2) + [(|\dot{\varepsilon}^{V}_{ij}|/C_2)^2 + 1]^{1/2}\}.$$

Similar expressions can be obtained for ε^{V}_{ij} (VV model) with N replaced by n_2 and F_b by F_a, Eq. (5). All the magnitude quantities are defined by the Tresca relation in order to be consistent with the previous experimental observation that the strain rate magnitudes defined by the Tresca relation are constant at any given time for those creep tests whose stresses are equal according to the Tresca relation.

The validity of these multiaxial relations can be checked by viewing the data and theory for the first step of each of the pure tension and the combined tension and torsion tests shown in Fig. 1-8. The dashed and dash-dot lines represent the results predicted by the above multiaxial relations for VV and VP models, respectively.

Since this paper deals only with multistep proportional loadings, $\dot{\varepsilon}^{V}_{ij}$ was taken to be zero whenever Σ_{ij} was smaller than zero, i.e. ε^{V}_{ij}

was frozen. More complicated stress histories will be discussed in subsequent papers.

PREDICTIONS BY THE THEORIES

In summary, two theoretical models are presented: VV and VP. In each model the time dependent nonrecoverable strain was represented by either the SH flow rule, Eq. (13), or by the KH flow rule, Eq. (33) and (34). Eq. (13) can be integrated explicitly for proportional loadings as shown by Eq. (19) for ε_{11}^{V}. The modified superposition principle was used for representing the viscoelastic component under variable stress states as shown by Eq. (8) for ε_{11}^{VE}. An IMSL subroutine DVERK based on the Runge-Kutta-Verner fifth and sixth order method with automatic time step control was used for the numerical integration.

The results are shown in Fig. 1-8 in which VV-SH are represented by solid lines, VP-SH by dotted lines, VV-KH by dashed lines, and VP-KH by dash-dot lines. The back stresses α_{ij} at the end of each step are shown in Table 2.

DISCUSSION

A comparison of the theoretical results with experimental data shows that both VV-SH and VV-KH give very good predictions of the material responses. Since the nonrecoverable strains were frozen in the KH models whenever Σ_{ij} was smaller than zero, VV-SH is better than VV-KH in some steps such as step 6 of Fig. 1. Adding a linear evolution rule for K_1 or K_2 in the KH rules was tried, but did not

result in a smaller α_{ij} at the beginning of these steps as required in order for the applied stress to induce further creep. This might be an inherent disadvantage for the state variable approach.

Since the ε^{VE} component was not included in either VP-SH or VP-KH, they could not predict the recovery strains and the transient creep strains upon reloadings such as observed in period 3 of Fig. 3 and 4, etc. Most of the work of other investigators based on VP models used a "static recovery" term (representing annealing after cold work) in the evolution rule to simulate the transient strains, see [18]. The present work shows that the ε^{VE} component can account for these behaviors without introducing annealing effects into the analysis.

CONCLUSIONS

A strain hardening (SH) and a kinematic hardening (KH) flow rule were developed from constant stress creep and recovery data. Both are in the form of a system of coupled ordinary differential equations. Under multistep proportional loadings, the strain hardening flow rules can be integrated explicitly to obtain all the strain components at any given time. Associated with each hardening rule, data are represented by two theoretical models: a viscous-viscoelastic (VV) model and a viscoplastic (VP) model. The viscoelastic components were represented by the modified superposition principle for both models. The agreements of the VV models with the experimental observations are generally very good. VV-SH is better than VV-KH in some step down stress states. The viscoelastic component is essential in accounting

for not only the recovery strain but also the transient creep strain upon reloadings and step up loadings.

ACKNOWLEDGEMENT

This work was supported by the Army Research Office, Research Grant Number DAAG29-81-K-0138. The material was contributed by the Aluminum Company of America. The authors are grateful to R. M. Reed for assistance in experiments and C. P. Capece for typing the manuscript.

REFERENCES

1. Findley, W.N., Cho, U.W., Ding, J.L., "Creep of Metals and Plastic Under Combined Stresses, A Review," ASME Journal of Engineering Materials and Technology, Vol. 101, 1979, p. 365.

2. Murakami, S., and Ohno, N., "A Constitutive Equation of Creep Based on the Concept of a Creep-Hardening Surface," Int. J. Solids Structures, Vol. 18, No. 7, 1982, pp. 597-609.

3. Ohashi, Y., Ohno, N., and Kawai, M., "Evaluation of Creep Constitutive Equations for Type 304 Stainless Steel Under Repeated Multiaxial Loading," ASME Journal of Engineering Materials and Technology, Vol. 104, 1982, pp. 159-164.

4. Kraus, H., Creep Analysis, Wiley, New York (1980).

5. Orowan, E., "The Creep of Metals," J. West Scot. Iron & Steel Inst., Vol. 54, 1946, pp. 45-53.

6. Miller, A.K., "An Inelastic Constitutive Model for Monotonic, Cyclic, and Creep Deformation: Part 1 - Equations Development and Analytical Procedures and Part 2 - Applications to Type 304 Stainless Steel," ASME Journal of Engineering Materials and Technology, Vol. 98, 1976, p. 97.

7. Kreig, R.D., Swearengen, J.C., and Rohde, R.W., "A Physically Based Internal Variable Model for Rate Dependent Plasticity," in "Inelastic Behavior of Pressure Vessel and Piping Components," PVP-PE-028(ASME), 1978, p. 15.

8. Hart, E.W., "Constitutive Relations for the Nonelastic Deformation of Metals," ASME Journal of Engineering Materials and Technology, Vol. 98, 1976, p. 193.

9. Findley, W.N., and Lai, J.S., "Creep and Recovery of 2618 Aluminum Alloy Under Combined Stress with a Representation by a Viscous-Viscoelastic Model," ASME Journal of Applied Mechanics, Vol. 45, Sept. 1978, pp. 507-514.

10. Lai, J.S., and Findley, W.N., "Creep of 2618 Aluminum Under Step Stress Changes Predicted by a Viscous-Viscoelastic Model," ASME Journal of Applied Mechanics, Vol. 47, Mar. 1980, pp. 21-26.

11. Findley, W.N., and Lai, J.S., "Creep of 2618 Aluminum Under Side Steps of Tension and Torsion and Stress Reversal Predicted by a Viscous-Viscoelastic Model," ASME Journal of Applied Mechanics, Vol. 48, 1981, pp. 47-54.

12. Lai, J.S., and Findley, W.N., "Simultaneous Stress Relaxation in Tension and Creep in Torsion of 2618 Aluminum at Elevated Temperature," ASME Journal of Applied Mechanics, Vol. 49, 1982, pp. 19-25.

13. Ding, J.L., and Findley, W.N., "48 Hour Multiaxial Creep and Recovery of 2618 Aluminum Alloy at 200°C," EMRL-87, Brown University, October, 1982.

14. Findley, W.N., and Gjelsvik, A., "A Biaxial Testing Machine for Plasticity, Creep or Relaxation Under Variable Principal Stress Ratios," Proceedings, American Society for Testing and Materials, Vol. 62, 1962, pp. 1103-1118.

15. Findley, W.N., "A Compressive Creep Machine," ASTM Journal of Testing and Evaluation, Vol. 10, July 1982, pp. 179-180.

16. Cho, U.W., and Findley, W.N., "Creep and Plastic Strains of 304 Stainless Steel at 593°C Under Step Stress Changes, Considering Aging," ASME Journal of Applied Mechanics, Vol. 49, 1982, pp. 297-304.

17. Findley, W.N., Lai, J.S., and Onaran, K., Nonlinear Creep and Relaxation of Viscoelastic Materials, With an Introduction to Linear Viscoelasticity, North-Holland, Amsterdam, 1976.

18. Matlock, D.K., Harrigan, W.C. Jr., and Nix, W.D., "On the Importance of Including Recovery in Phenomenological Theories of Plastic Flow in Metal," Acta Metallurgica, Vol. 20, 1972, pp. 661-668.

Table 1: Results used for estimation of the "early" shear creep rates

TEST NO.	SHEAR STRESS,		ε_{12}^{+V}, (in Eq. (1) with $n_1 = 0.223$, $n_2 = 0.330$)	ε_{12}^{+}, (in Eq. (2) with $N = 0.292$)	$\dot{\varepsilon}_{12}^{V}$ at $t = 0$, (from $n_2 \varepsilon_{12}^{+V} t_1^{n_2-1}$, $t_1 = 1$ sec)	$\dot{\varepsilon}_{12}^{V}$ at $t = 0$, (from $N \varepsilon_{12}^{+} t_1^{N-1}$ $t_1 = 1$ sec)
	MPa	(ksi)	$10^{-4}/h^{n_2}$	$10^{-4}/h^{N}$	$10^{-2}/h$	$10^{-2}/h$
T28	27.4	(3.97)	0.1417	0.3592	0.1129	0.3456
T29	41.4	(6.00)	0.3629	0.6608	0.2891	0.6358
T26	63.2	(9.17)	1.034	1.699	0.8237	1.635
T38	79.2	(11.49)	2.404	3.514	1.915	3.381
T42	101.4	(14.70)	7.544	9.564	6.009	9.202

Table 2: Applied stress deviator (σ'_{ij}) in each period and back stress (α_{ij}) at the end of the period.

TEST NO.	STRESS, MPa	PERIOD									
		1	2	3	4	5	6	7	8	9	10
T23	σ'_{12}	27.579	0.000	27.600	13.790	55.158	41.369	27.600	13.790	0.000	
	α_{12}(VV)	27.547	27.547	27.553	27.553	55.024	55.024	55.024	55.024	55.024	
	α_{12}(VP)	27.565	27.565	27.568	27.568	55.096	55.096	55.096	55.096	55.096	
A24	σ'_{11}	55.158	0.000	27.579	41.369	55.158	41.369	27.579	0.000		
	α_{11}(VV)	55.084	55.084	55.084	55.084	55.098	55.098	55.098	55.098		
	α_{11}(VP)	55.125	55.125	55.125	55.125	55.132	55.132	55.132	55.132		
A25	σ'_{11}	41.369	0.000	41.369	27.579	13.790	0.000	13.790	27.579	41.369	0.000
	α_{11}(VV)	41.319	41.319	41.328	41.328	41.328	41.328	41.328	41.328	41.334	41.334
	α_{11}(VP)	41.346	41.346	41.351	41.351	41.351	41.351	41.351	41.351	41.354	41.354
T26	σ'_{12}	63.200	0.000	63.200	31.600	63.200	31.600	0.000			
	α_{12}(VV)	63.057	63.057	63.082	63.082	63.097	63.097	63.097			
	α_{12}(VP)	63.134	63.134	63.146	63.146	63.153	63.153	63.153			
CA31	σ'_{11}	55.158	0.000	55.158	27.579	0.000	55.158	36.772	18.386	0.000	
	α_{11}(VV)	55.056	55.056	55.123	55.123	55.123	55.086	55.086	55.086	55.086	
	α_{11}(VP)	55.114	55.114	55.075	55.075	55.075	55.129	55.129	55.129	55.129	
CT31	σ'_{12}	41.369	0.000	41.369	20.684	0.000	41.369	27.579	13.790	0.000	
	α_{12}(VV)	41.292	41.292	41.306	41.306	41.306	41.315	41.315	41.315	41.315	
	α_{12}(VP)	41.335	41.335	41.342	41.342	41.342	41.347	41.347	41.347	41.347	
A32 and A37*	σ'_{11}	72.970	0.000	72.970	36.485	0.000	72.970	48.647	24.323	0.000	
	α_{11}(VV)	72.846	72.846	72.869	72.869	72.869	72.883	72.883	72.883	72.883	
	α_{11}(VP)	72.915	72.915	72.927	72.927	72.927	72.934	72.934	72.934	72.934	
A44*	σ'_{11}	91.471	0.000	91.471	60.980	30.490	0.000	45.736	91.471	45.736	0.000
	α_{11}(VV)	91.240	91.240	91.283	91.283	91.283	91.283	91.283	91.308	91.308	91.308
	α_{11}(VP)	91.375	91.375	91.396	91.396	91.396	91.396	91.396	91.408	91.408	91.408

*Compression test

Note: 1. In pure tension tests, $\alpha_{ij} = 0$ except $\alpha_{22} = \alpha_{33} = -(1/2)\alpha_{11} \neq 0$

2. In pure torsion tests, $\alpha_{ij} = 0$ except $\alpha_{12} = \alpha_{21} \neq 0$

3. In combined tension and torsion tests, $\alpha_{ij} = 0$ except $\alpha_{12} = \alpha_{21} \neq 0$, $\alpha_{22} = \alpha_{33} = -(1/2)\alpha_{11} \neq 0$

FIGURE CAPTIONS

Fig. 1: Test T23. X = 8 h, Y = 0.02%. Numbers in parenthesis on the ordinate indicate the creep period to which the ordinate number applies. Solid lines: Viscous-viscoelastic with strain hardening; Dashed lines: Viscous-viscoelastic with kinematic hardening; Dotted lines: Viscoplastic with strain hardening; Dot-dashed lines: Viscoplastic with kinematic hardening.

Fig. 2: Test A24. X = 8 h, Y = 0.02%. See caption of Fig. 1 for key to theory curves.

Fig. 3: Test A25. X = 8 h, Y = 0.02%. Numbers in parenthesis on the ordinate indicate the creep period to which the ordinate number applies. See caption of Fig. 1 for key to theory curves.

Fig. 4: Test T26. X = 8 h, Y = 0.02%. Numbers in parenthesis on the ordinate indicate the creep period to which the ordinate number applies. See caption of Fig. 1 for key to theory curves.

Fig. 5: Test CA31. X = 8 h, Y = 0.02%. Numbers in parenthesis on the ordinate indicate the creep period to which the ordinate number applies. See caption of Fig. 1 for key to theory curves.

Fig. 6: Test CT31. X = 8 h, Y = 0.02%. Numbers in parenthesis on the ordinate indicate the creep period to which the ordinate number applies. See caption of Fig. 1 for key to theory curves.

Fig. 7: Tests A32, a tension creep test, and A37, a compression creep test (designated by COMP). X = 8 h, Y = 0.02%. Numbers in parenthesis on the ordinate indicate the creep period to which the ordinate number applies. See caption of Fig. 1 for key to theory curves.

Fig. 8: Test A44, a compression creep test. X = 8 h, Y = 0.04%. Numbers in parenthesis on the ordinate indicate the creep period to which the ordinate number applies. See caption of Fig. 1 for key to theory curves.

Fig. 9: Early shear rates vs. shear stresses.

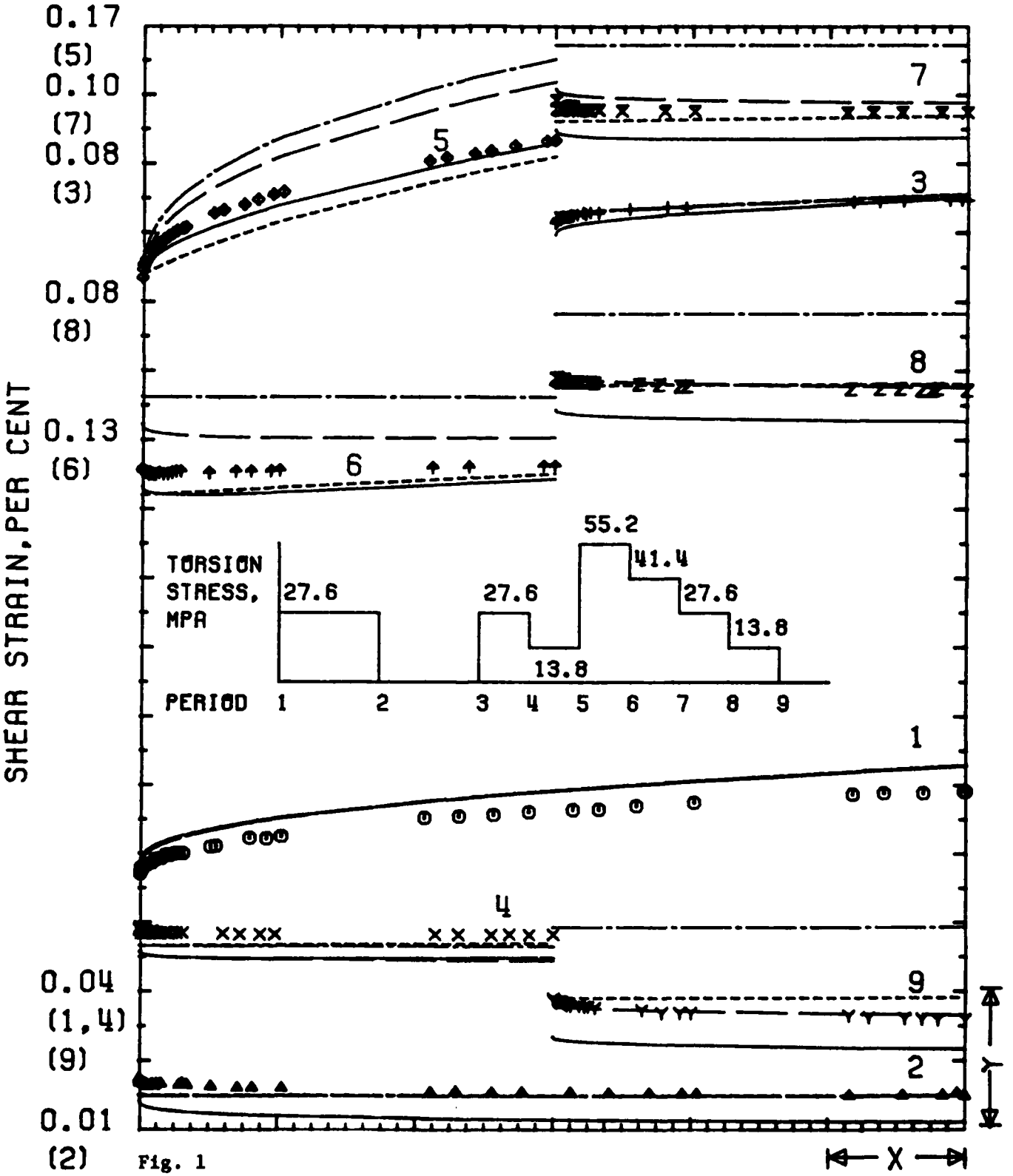
0.17
(5)
0.10
(7)
0.08
(3)
0.08
(8)
0.13
(6)
0.04
(1,4)
(9)
0.01
(2)
SHEAR STRAIN, PER CENT
TIME, HOURS
X
Y
1
2
3
4
5
6
7
8
9
TORSION STRESS, MPA
PERIOD
27.6
27.6
55.2
41.4
27.6
13.8
13.8
1
2
3
4
5
6
7
8
9

Fig. 1

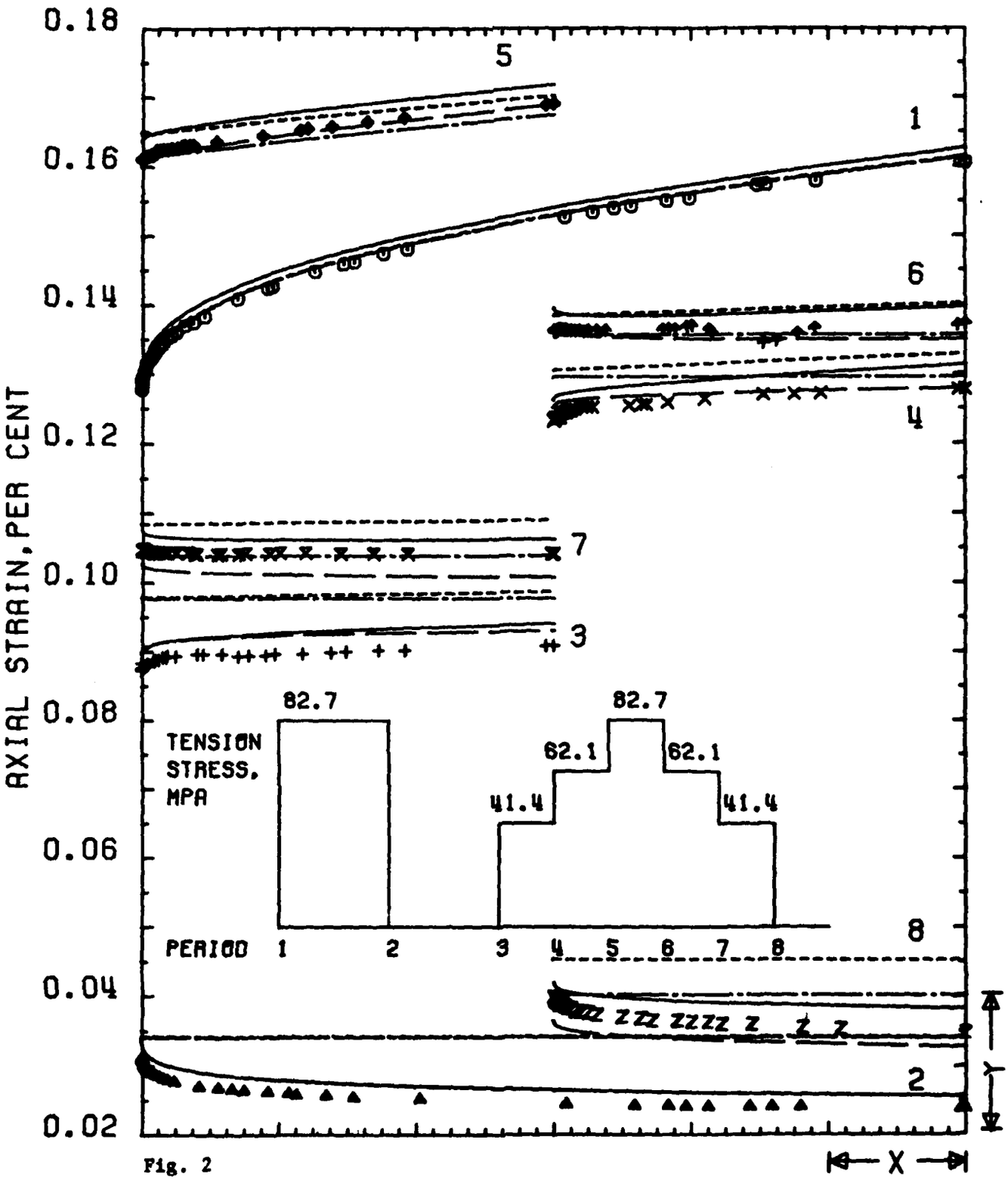
0.18
0.16
0.14
0.12
0.10
0.08
0.06
0.04
0.02
AXIAL STRAIN, PER CENT
5
1
6
4
7
3
8
2
TENSION STRESS, MPA
82.7
82.7
62.1
62.1
41.4
41.4
PERIOD 1 2 3 4 5 6 7 8
Y
X
TIME, HOURS

Fig. 2

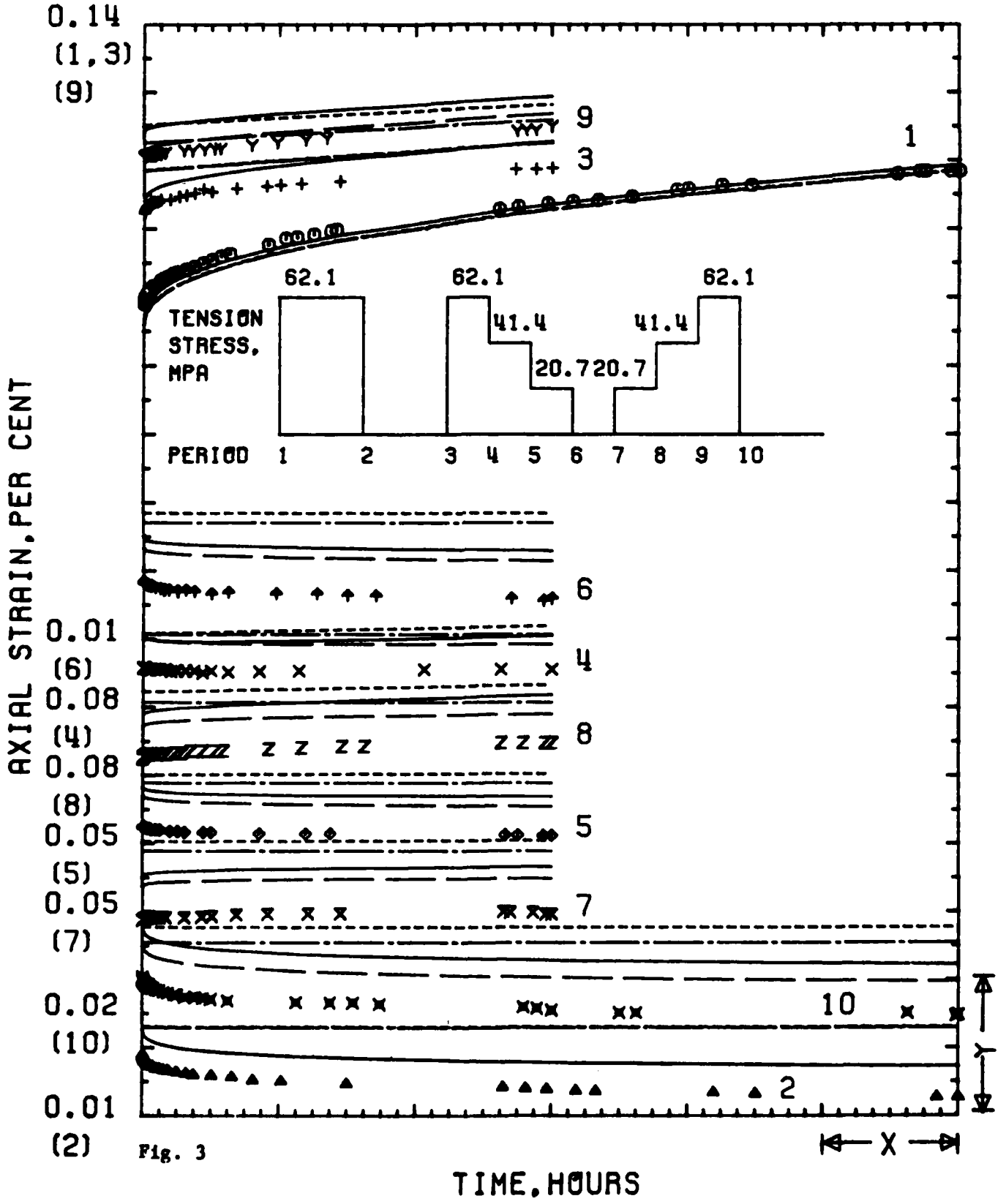
0.14
(1,3)
(9)
9
3
1
62.1
62.1
62.1
TENSION
STRESS,
MPA
41.4
41.4
20.7
20.7
PERIOD 1 2 3 4 5 6 7 8 9 10
6
0.01
(6)
4
0.08
(4)
8
0.08
(8)
0.05
(5)
5
0.05
(7)
7
0.02
(10)
10
0.01
(2)
2
AXIAL STRAIN, PER CENT
Y
X
TIME, HOURS

Fig. 3

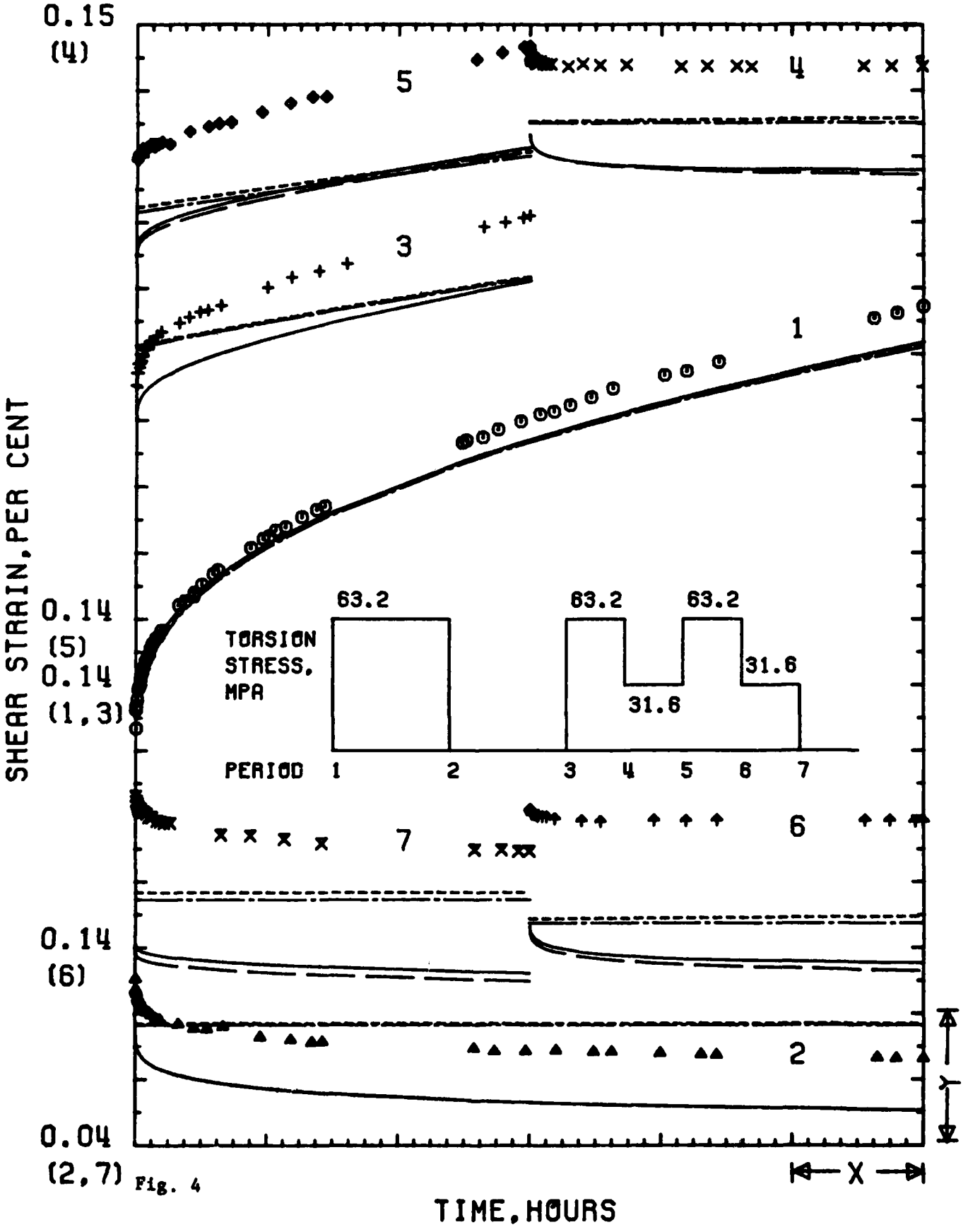
0.15
(4)
0.14
(5)
0.14
(1,3)
0.14
(6)
0.04
(2,7)
SHEAR STRAIN, PER CENT
TIME, HOURS
TORSION STRESS, MPA
63.2
63.2
63.2
31.6
31.6
PERIOD 1 2 3 4 5 6 7
1
2
3
4
5
6
7
X
Y

Fig. 4

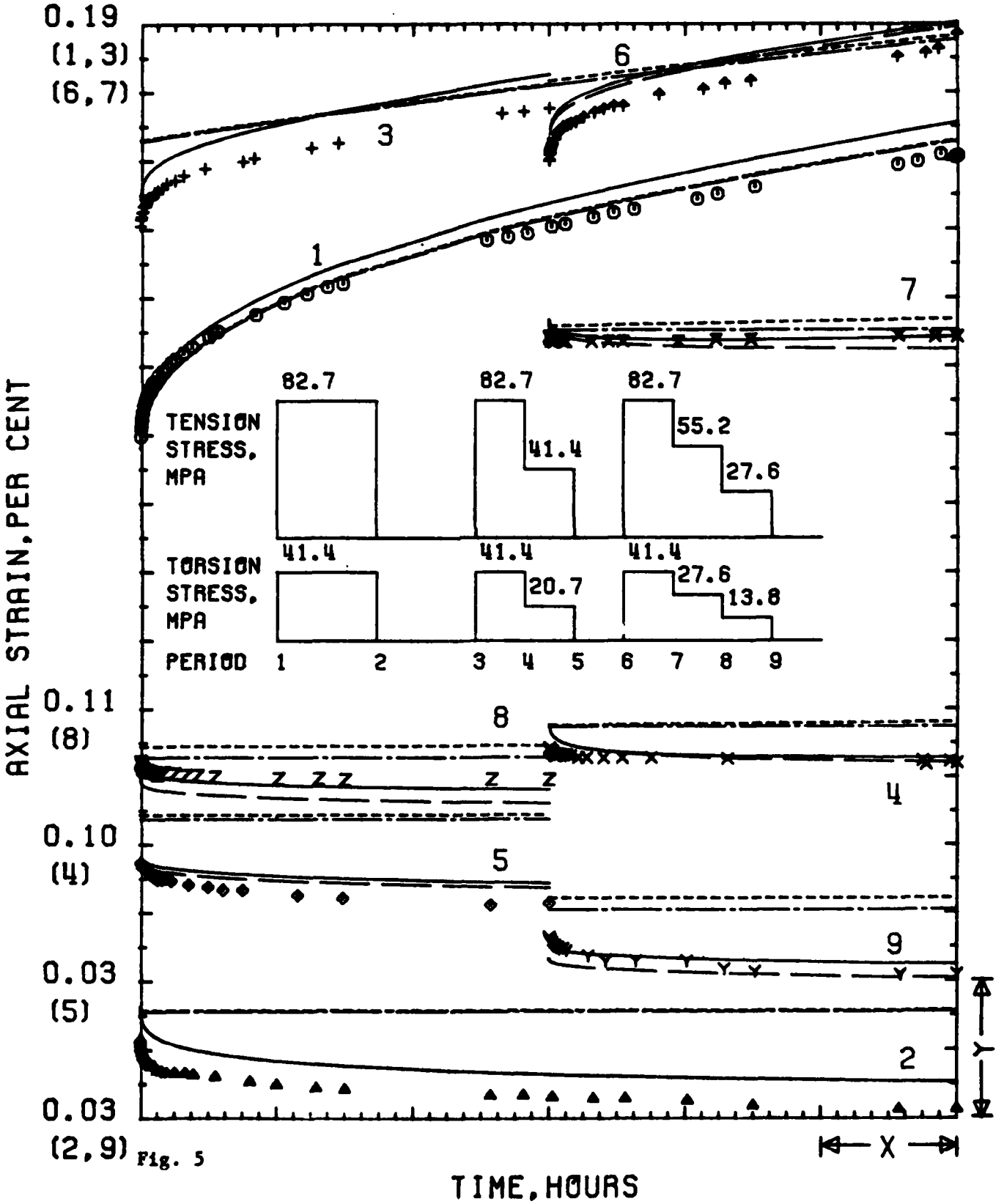
0.19
(1,3)
(6,7)
0.11
(8)
0.10
(4)
0.03
(5)
0.03
(2,9)
AXIAL STRAIN, PER CENT
6
3
1
7
8
4
5
9
2
82.7
82.7
82.7
TENSION STRESS, MPA
41.4
55.2
27.6
41.4
41.4
41.4
TORSION STRESS, MPA
20.7
27.6
13.8
PERIOD 1 2 3 4 5 6 7 8 9
Y
X
TIME, HOURS

Fig. 5

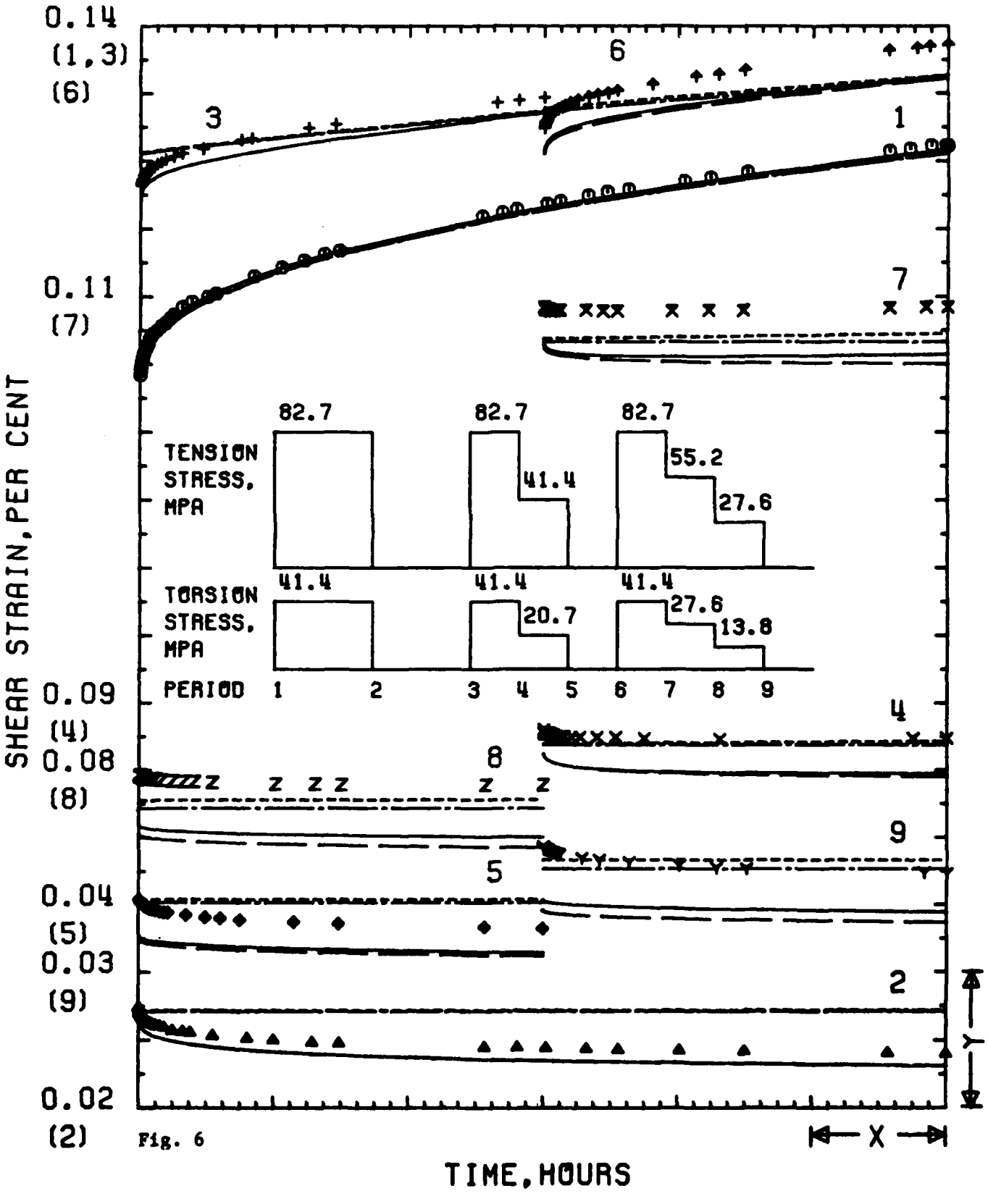
0.14
(1,3)
(6)
0.11
(7)
0.09
(4)
0.08
(8)
0.04
(5)
0.03
(9)
0.02
(2)
SHEAR STRAIN, PER CENT
TENSION STRESS, MPA
82.7
82.7
82.7
41.4
55.2
27.6
TORSION STRESS, MPA
41.4
41.4
41.4
20.7
27.6
13.8
PERIOD
1
2
3
4
5
6
7
8
9
1
2
3
4
5
6
7
8
9
Y
X
TIME, HOURS

Fig. 6

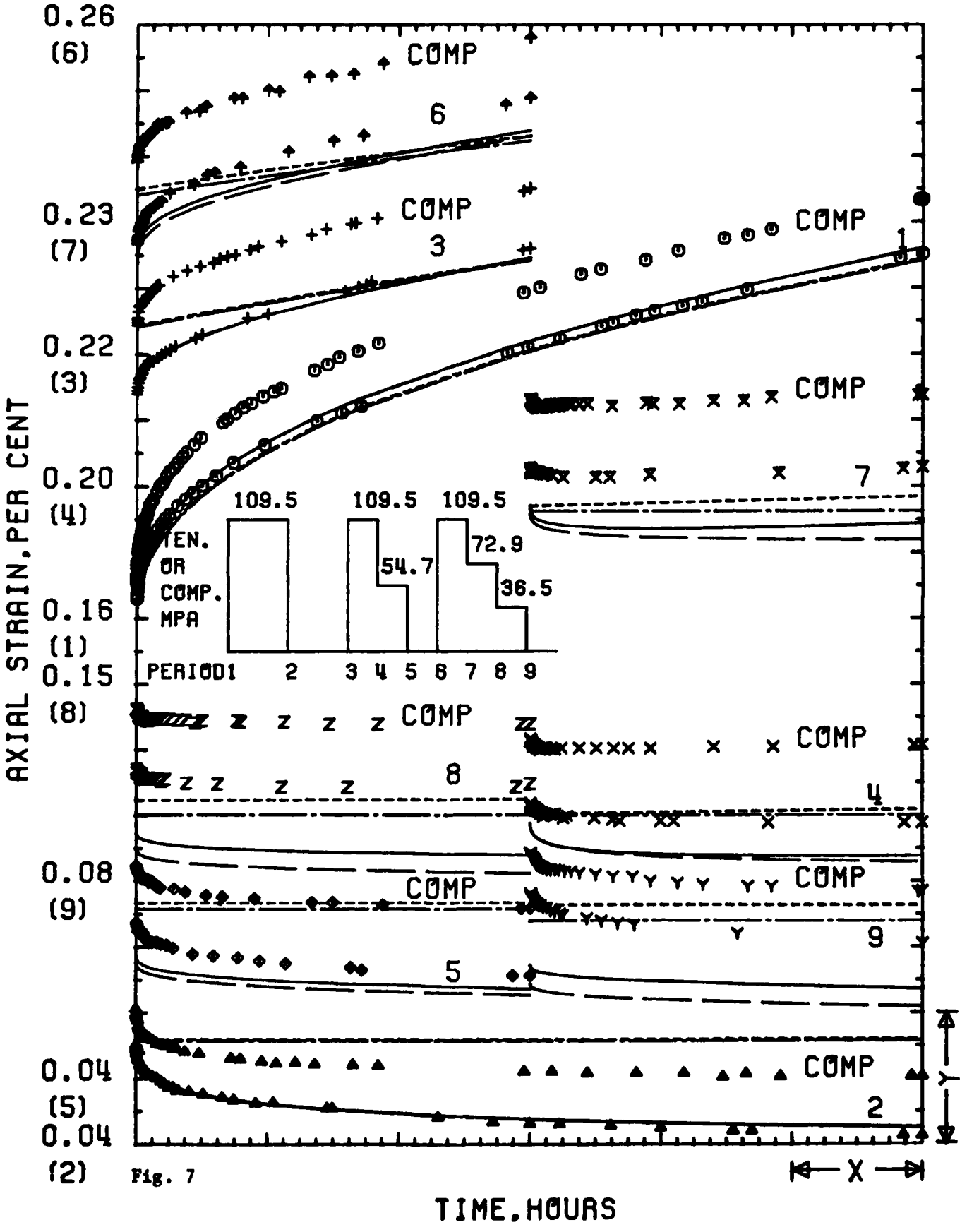
0.26
(6)
0.23
(7)
0.22
(3)
0.20
(4)
0.16
(1)
0.15
(8)
0.08
(9)
0.04
(5)
0.04
(2)
AXIAL STRAIN, PER CENT
COMP
6
COMP
3
COMP
1
COMP
7
109.5
109.5
109.5
72.9
54.7
36.5
TEN.
OR
COMP.
MPA
PERIOD 1 2 3 4 5 6 7 8 9
COMP
8
COMP
4
COMP
9
COMP
5
COMP
2
Y
X
TIME, HOURS

Fig. 7

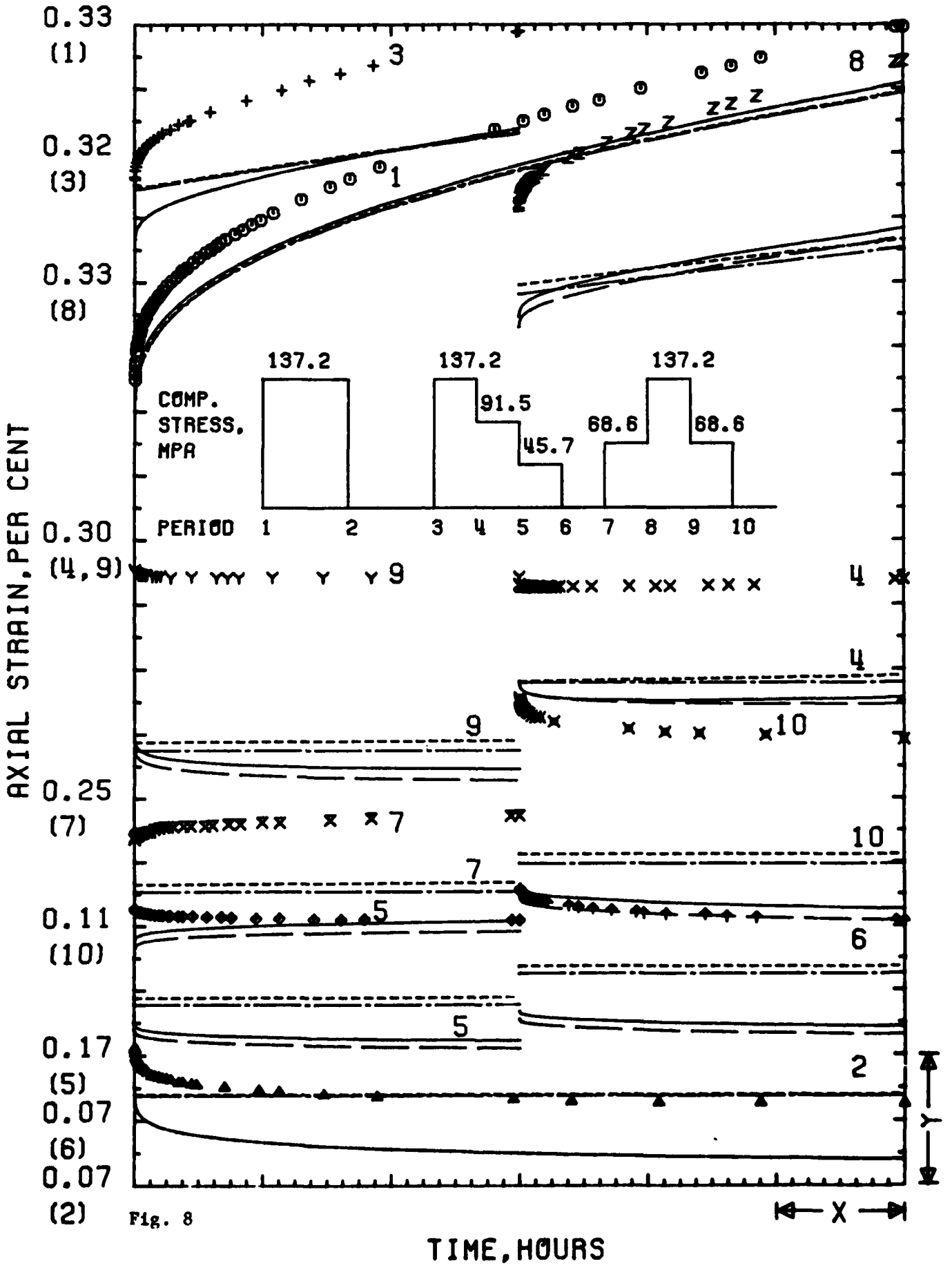
0.33
(1)
0.32
(3)
0.33
(8)
0.30
(4,9)
0.25
(7)
0.11
(10)
0.17
(5)
0.07
(6)
0.07
(2)
AXIAL STRAIN, PER CENT
137.2
137.2
137.2
91.5
45.7
68.6
68.6
COMP. STRESS, MPA
PERIOD 1 2 3 4 5 6 7 8 9 10
1
2
3
4
5
6
7
8
9
10
Y
X
TIME, HOURS

Fig. 8

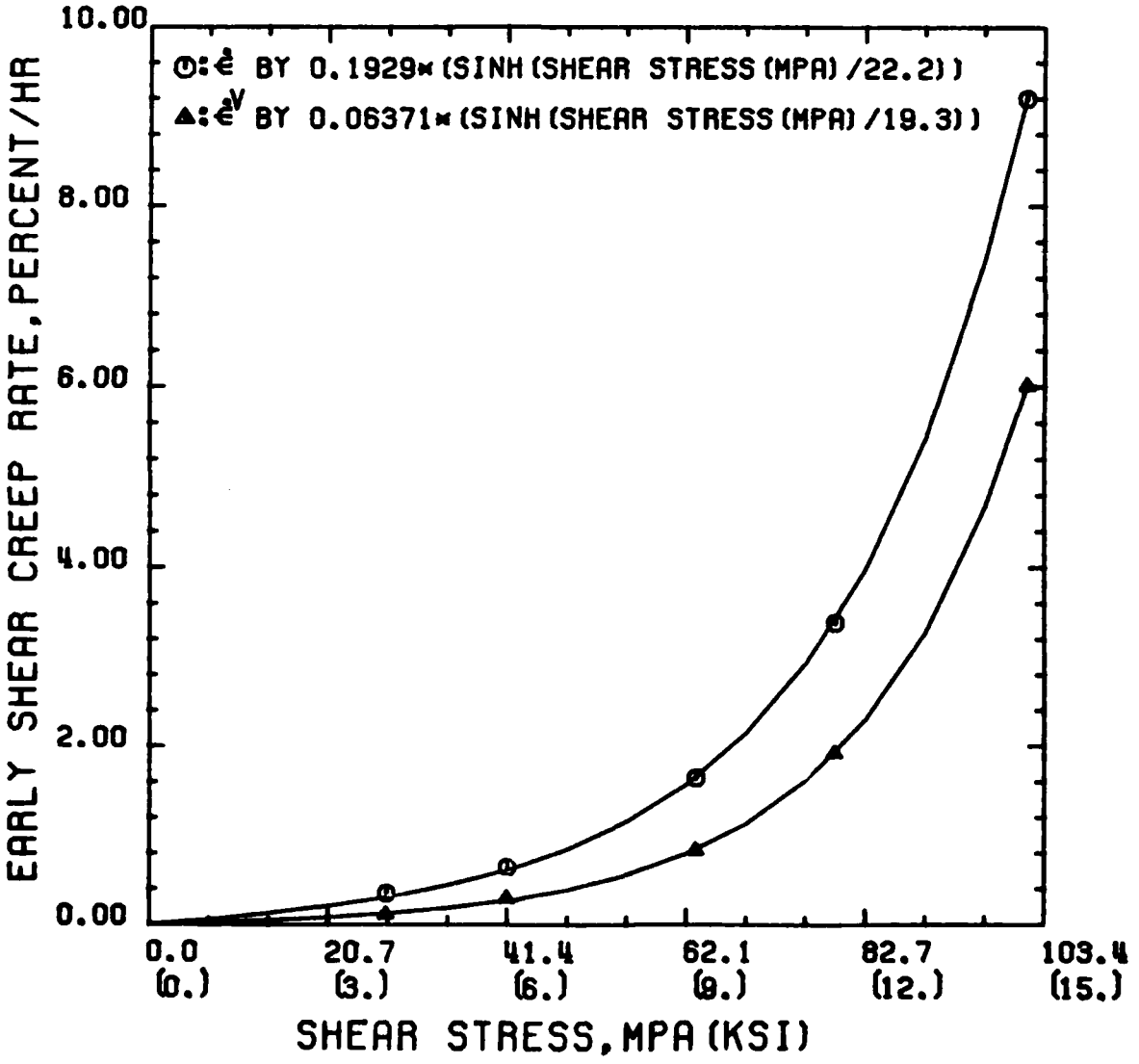
10.00
8.00
6.00
4.00
2.00
0.00
EARLY SHEAR CREEP RATE, PERCENT/HR
⊙: $\dot{\epsilon}$ BY 0.1929* (SINH (SHEAR STRESS (MPA) /22.2))
▲: $\dot{\epsilon}^{v}$ BY 0.06371* (SINH (SHEAR STRESS (MPA) /19.3))
0.0 (0.)
20.7 (3.)
41.4 (6.)
62.1 (9.)
82.7 (12.)
103.4 (15.)
SHEAR STRESS, MPA (KSI)

Fig. 9

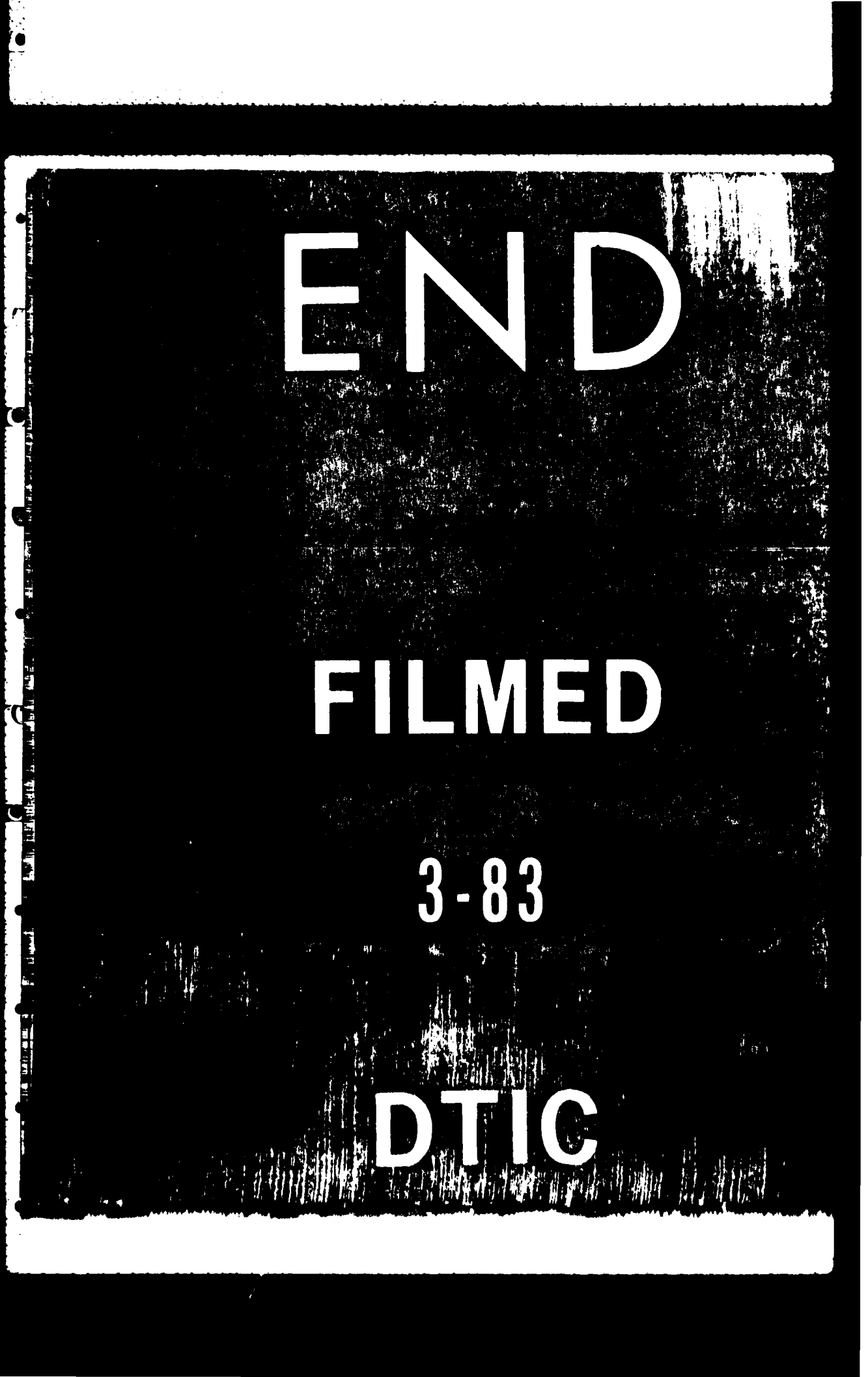
END
FILMED
3-83
DTIC